J. Chem. Sci. (2025)137:113
https://doi.org/10.1007/s12039-025-02432-4

REGULAR ARTICLE

Modulating magnetic exchange and magnetic anisotropy in {3d–4f} complexes using external electric field

TANU SHARMA and GOPALAN RAJARAMAN*
Department of Chemistry, Indian Institute of Technology Bombay, Mumbai 400 076, India
*Corresponding Author. E-mail: rajaraman@chem.iitb.ac.in

MS received 8 March 2025; revised 27 May 2025; accepted 2 July 2025

Abstract. One of the holy grails in the area of single-molecule magnets (SMMs) is to achieve control over microscopic spin Hamiltonian parameters of molecules, and this is generally achieved via chemical intuition, serendipity, and occasionally using external stimuli such as pressure. Among the spin Hamiltonian parameters that control the performance of SMMs, magnetic exchange coupling and magnetic anisotropy are the key parameters that can be controlled via chemical design, which is challengingactive space self-consistent. In this work, we have explored using a combination of density functional theory (DFT) and *ab initio* CASSCF/RASSI-SO method in combination with the response theory method wherein an external electric field was applied to effect controlled geometric changes that, in turn, were found to alter both the magnetic exchange and magnetic anisotropy in a {Ln-Cr} (Ln= Gd^{III} and Dy^{III}) molecule. Particularly, here we studied $[CrF_2(py)_4]Ln(hfac)_4]$ (Ln = Gd (**1**) and Dy^{III} (**2**)) molecule possessing antiferromagnetic coupling between Gd^{III}…Cr^{III} using an oriented external electric field, and our study reveals that application of field 0.4 to 2 V/Å along the Cr–F and Gd–F directions alter the geometry, and this, in turn, alters the *J* and the associated magnetic anisotropy. As this *J* is weakly antiferromagnetic, our aim was to apply electric field to reduce the anti-ferromagnetic coupling and see if it is possible to alter the magnitude of magnetic coupling. Applying an oriented external electric field (OEEF) along the ± *x*-axis led to significant elongation of the Gd−F bond distance, increasing from 2.349 Å in the absence of a field to 2.864 Å at ± 2 V/Å. This structural modification resulted in a notable reduction of the antiferromagnetic *J*, decreasing from −0.960 cm^{-1} in the ground state of **1** to −0.100 cm^{-1} at +2 V/Å, corresponding to an approximate 90% decrease. Conversely, applying the OEEF along the ± *z*-axis induced negligible changes in both the Gd−F bond distance and the exchange coupling constant. Although the sign change was not achieved, this suggests a viable way to alter the magnetic exchange. For the corresponding Dy^{III} analogues, our calculations indicate that the corresponding geometrical distortions, particularly shorter Dy-F distance at the applied field strength of 0.4 to 2 V/Å, enhance the magnetic anisotropy and eventually yield better performing SMMs. These findings align with experimental observations reported in the literature, where electric fields have been shown to modulate magnetic exchange interactions in molecular systems. Our results demonstrate the potential of using external electric fields to tailor magnetic properties in {3d–4f} complexes, thereby advancing the design of materials with controllable magnetic behaviours.

Keywords. Oriented external electric field; exchange coupling; 3d–4f complexes; magnetic anisotropy.

1. Introduction

Exchange interactions in 3d–4f molecular complexes exhibit remarkable sensitivity to structural modifications,[1–3] traditionally controlled through chemical means by altering ligand fields.[4–9] However, the application of oriented external electric fields (OEEFs)[10] represents a promising non-chemical alternative for modulating these interactions. This approach aligns with growing interest in physical methods for property control, including pressure, light, temperature, and electric field-based techniques. Magnetic exchange coupling (*J*) fundamentally determines the behaviour of single-molecule magnets

This article is part of the Special Issue on "Understanding Molecules to Materials at Different Length and Time Scales".

Supplementary Information: The online version contains supplementary material available at https://doi.org/10.1007/s12039-025-02432-4.

Published online: 02 December 2025

(SMMs). While factors such as bridging ligand type, bond geometries, and other structural parameters influence *J*, chemical modifications often present significant synthetic challenges. This limitation has driven the exploration of alternative approaches, with electric field modulation emerging as particularly promising due to its precision and versatility.

Unlike pressure-induced methods that face reproducibility challenges,[11–13] OEEFs offer more controlled manipulation of exchange interactions through subtle electronic structure modifications.[14] Experimental evidence increasingly supports the efficacy of electric fields in modulating magnetic exchange properties.[14–17] Electric fields provide superior spatial resolution compared to magnetic fields, enabling precise control over electron spin interactions.[10,14,16–18] Despite confirming that electric fields can influence both magnetic anisotropy and exchange interactions, a comprehensive understanding of structure-property relationships under electric field influence remains incomplete.

Lanthanide-based SMMs,[19–21] despite their high blocking temperatures, suffer from zero-field tunnelling effects that can be mitigated through magnetic exchange interactions. Unlike single-ion magnets (SIMs), where magnetic relaxation is primarily governed by the single-ion anisotropy of the paramagnetic metal centre, multinuclear systems rely on the anisotropy of the exchange-coupled states. In such systems, the presence of appropriate exchange coupling can generate an internal static magnetic field, effectively mimicking an externally applied field and significantly suppressing quantum tunnelling of magnetization (QTM). However, these systems typically exhibit weak, predominantly antiferromagnetic coupling.[22,23] This necessitates the exploration of external stimuli capable of enhancing and potentially reversing exchange interactions. Our study systematically analyses Gd–Cr complexes under electric field influence using density functional theory (DFT) and *ab initio* CASSCF calculations to establish principles governing exchange sign reversal and develop practical strategies for fine-tuning exchange without chemical modifications.

We selected the [trans-$[CrF_2(py)_4]Gd(hfac)_4]^7$ (**1**) (Figure 1(a)) complex[24,25] for its demonstrated sensitivity to external electric fields, particularly regarding Gd–Cr exchange interactions. OEEF application along specific molecular axes can modify electronic structures and bonding patterns, altering both the strength and sign of *J*. This electric field manipulation offers several advantages for quantum computing and spintronics applications, including precise spatial and temporal control, faster response compared to thermal methods, lower energy requirements, improved solid-state device compatibility, and potential for miniaturization. Recent research has demonstrated electric fields' diverse influences on molecular properties, from magnetization barriers in SMMs to chemical transformations and spin transitions. Our work aims to provide deeper insights into leveraging external electric fields for controlling 3d–4f complex magnetic properties, establishing fundamental principles for OEEF-based exchange modulation, developing approaches for achieving enhanced *J* values, and demonstrating feasible electric field control over 3d–4f exchange interactions. These findings will contribute significantly to electric field-based molecular magnet manipulation, offering new perspectives for designing high-performance SMMs for quantum computing, molecular spintronics, and information storage technologies. Specifically, we seek to unravel the following compelling questions. (i) How does OEEF influence the structural parameters crucial for regulating *J* values? (ii) To what extent does the nature of the co-ligand affect the control of magnetic exchange? (iii) Can OEEF be utilized to reverse the sign of magnetic exchange? (iv) Can this study be extended from isotropic Gd^{III} complexes to anisotropic Dy^{III} complexes to enhance SMM performance?

2. Computational details

Geometry optimizations were performed using DFT calculations implemented in the Gaussian 09 software package,[26] employing the hybrid B3LYP functional.[27–29] For Gd^{III} atoms, the CSDZ basis set[30] was chosen due to its precision in representing the electron distribution and interactions characteristic of these heavy elements. Cr^{III} atoms were treated with the SDD basis set,[31] which is suitable for transition metals and provides a good balance between computational efficiency and accuracy. The 6-31G* basis set was used for all other atoms in the study to ensure a reasonable compromise between accuracy and computational demand. This was implemented using the field keyword in the Gaussian 09 software[26], allowing for precise control over the electric field's intensity and direction. The application of the OEEF is crucial for studying its effects on the molecular structure and magnetic properties, as electric fields can induce significant structural modifications that influence magnetic interactions. Electric fields ranging from 2 V/Å to −2 V/Å were applied in both the *x* and *z* directions to investigate their effects on the spin densities and structural parameters of the complex (optimised coordinates are provided in Supplementary

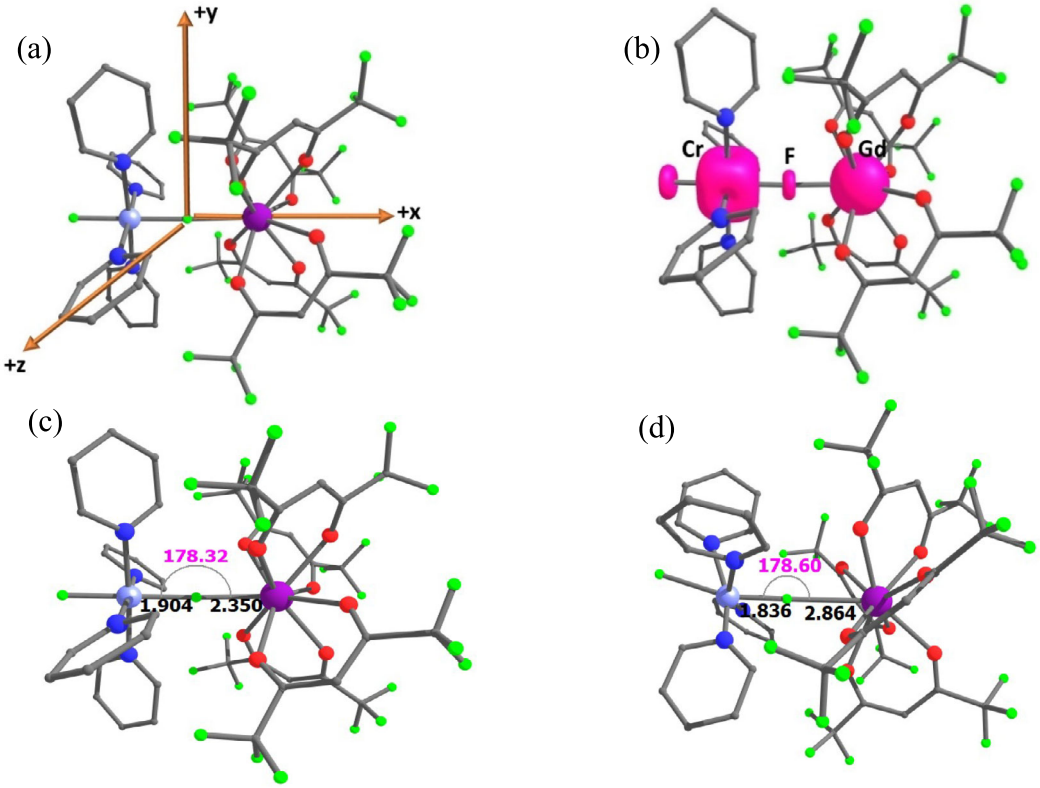

Figure 1. DFT optimized structures of (**a**) **1**(*trans*-[$CrF_2(py)_4$]Gd(hfac)$_4$) with axes, (**b**) spin density plot of **1**, (**c**) DFT optimized structure of **1** with the important structural parameters shown and (**d**) DFT optimized structure of $\mathbf{1}_{x+2}$ with the important structural parameters shown in colour code: purple, Gd; red, O; blue, N; green; light grey, C; light blue, Cr; green, F. Here hydrogens have been omitted for clarity. Magenta coloured surface shows the spin density present.

Information). Here, we used the notation $\mathbf{1}_{\mathbf{z+0.1}}$, which denotes the geometry of molecule **1** when 0.1 V/Å OEEF is applied along the +Z-direction. The electrostatic potential (ESP) diagram was generated using the same level of theory and basis sets as employed in the single-point energy calculations. The ESP was computed on a 0.05 e/Bohr^3 electron density isosurface and subsequently mapped onto the molecular surface, with the colour scale ranging from negative (magenta) to positive (blue) electrostatic potential values.

To determine the exchange coupling constants, Noodleman broken symmetry[31] method was employed. This method is particularly effective for studying magnetic systems as it accurately calculates exchange interactions by comparing high-spin and broken symmetry states. The CSDZ basis set[30] was again used for Gd^{III} to maintain consistency and accuracy, while the TZV basis set was employed for the remaining atoms.

Two spin states were computed: one high-spin state and the other, broken symmetry state. This dual-state computation helps to elucidate the nature of magnetic coupling under different electronic configurations. This thorough analysis allows for a deeper understanding of the magnetic interactions within this molecule. The Hamiltonian used is,

$$\hat{H} = -2J S_{Cr}.S_{Gd}$$

In this context, S_{Gd} and S_{Cr} represent the spins associated with Gd^{III} and Cr^{III}, which are 7/2 and 3/2, respectively. The symbol J denotes the isotropic exchange coupling constant, where positive J values indicate ferromagnetic coupling and negative J values indicate antiferromagnetic coupling. The magnetic anisotropy, spin relaxation energy barriers, and g-tensors were determined from first principles using the MOLCAS 8.2 software suite.[32] We have replaced the Gd^{III} with Dy^{III} for the single-ion anisotropy calculations. For Dy^{III}, the ANO-RCC-VTZP basis set[33] was employed to achieve high accuracy in representing the electronic structure. For all other elements, the ANO-RCC VDZP basis set was used. The Douglas–Kroll–Hess (DKH) Hamiltonian[34] was applied to incorporate the relativistic effects that are significant in heavy metal centres such as lanthanides.

In the complete active space self-consistent field (CASSCF)[35] calculations, seven Ln^{III} orbitals were selected as active spaces, with guess orbitals generated beforehand to facilitate the calculations. Spin-free energies were obtained via CASSCF, and these energies were further refined using restricted active space state interaction with spin-orbit coupling (RASSI-SO) to generate spin-orbit coupled states from 21 sextets. The g-tensors were then extracted using the SINGLE_ANISO module.[36] To manage the computational demands, disk usage was optimised through Cholesky decomposition, a technique that reduces the memory and storage requirements without sacrificing accuracy.

3. Results and Discussion

We have performed DFT calculations combined with *ab initio* calculations in the presence of an OEEF. The magnetic properties of lanthanide SMMs are highly sensitive to geometric variations, including bond lengths and angles. To investigate the impact of an external electric field on structural parameters, we applied the field along the –X and –Z directions, where –X corresponds to alterations in the F–Cr bond, +X influences the F–Gd bond, and –Z is perpendicular to the Cr–F–Gd axis. The field was incrementally increased in both positive and negative directions until noticeable geometric distortions occurred, and the resulting changes in bond lengths and angles were systematically analysed. Additionally, calculations were performed on modified ligand environments to assess their influence on key structural parameters. This approach specifically aims to explore how the F-linker responds to external perturbations, providing insights into its role in governing the system's overall structural and magnetic behaviour.

The application of an external electric field along the X and Z directions induces significant geometric modifications in the Cr–F–Gd system, with varying effects on bond lengths and angles depending on the OEEF field magnitude and direction. The spin densities measured were ~7.010 on Gd^{III} and 2.920 on Cr^{III}, with an exchange coupling constant of $-0.960\ cm^{-1}$, consistent observations with experimental (Figure 1(b)) across all optimised geometries of the complex. However, significant structural differences were observed in the electric field-modulated structures, as detailed in Table 1. Despite the application of varying electric fields, the spin densities remained consistent.

The Cr–F (terminal) bond elongates with increasing field strength along +X, reaching 1.868 Å at +2 V/Å, a 1.3% increase from its original value of 1.844 Å. In contrast, applying the field along –X results in relatively minor changes, with a maximum deviation of 0.27% at −2 V/Å. Along the Z direction, the response is stronger for +Z, where the bond increases by 2.12% at +2 V/Å, while under −Z, the variation remains minimal. The Cr–F (bridged) bond exhibits moderate sensitivity, contracting under +X with a 3.57% decrease at +2 V/Å, whereas under −X, it remains relatively stable with deviations below 1.4%. Along Z, this bond elongates under −Z and contracts under +Z, with a maximum 2.9% reduction at +2 V/Å. The F–Gd bond experiences the most pronounced changes, particularly under the –X and −Z fields. In the +X direction, it increases slightly, reaching 2.524 Å (+7.44%) at +1 V/Å and 2.864 Å (+21.91%) at +2 V/Å. However, under –X, a dramatic elongation occurs, extending to 3.442 Å at –2 V/Å, representing a 46.6% increase and suggesting a significant weakening of the bond. A similar trend is observed under the Z field, with the bond stretching by 34.2% (3.343 Å) at −2 V/Å while remaining relatively stable under moderate fields.

The F–Cr–F bond angle is fairly robust, particularly in the Z direction, where it stabilizes at 179.9° across all field strengths. Under +X and –X, a minor decrease is observed, reaching 173.7° at −2 V/Å, a 3.0% reduction. The Cr–F–Gd angle remains relatively stable under small and moderate fields, varying within ±1% of its original value, highlighting its robustness to external perturbations. Comparing the effects along X and Z directions, the X field primarily alters F–Cr and F–Gd bond lengths, with stronger effects in the negative direction (−X), leading to substantial F–Gd elongation. In contrast, the Z field significantly affects both Cr–F bonds, particularly the bridged Cr–F bond, while F–Gd elongates predominantly under –Z. The positive and negative fields do not produce symmetric effects; for instance, both +X and –X increase F–Gd, but the elongation under –X is considerably larger. Similarly, +Z leads to bond contraction, whereas –Z causes elongation, especially for F–Gd.

Previous studies have highlighted the critical role of the Gd−F−Cr angle in determining the exchange behaviour between Gd^{III} and Cr^{III} in such complexes. However, the application of OEEF resulted in negligible changes to Gd−F−Cr angles in both the $\pm x$ and $\pm z$ directions, as shown in Table 1, Figures 1(c), (d) and 2(a). Figure 2(a) shows the $\Delta(\angle CrFGd_{mol} - \angle CrFGd_{mol\pm n})$, and it shows the maximum change in ∠CrFGd occurs at −1 and −2 V/Å. Interestingly, the Gd−F bond distance exhibited notable changes when subjected to OEEF in the $\pm x$ and $\pm z$ directions (Table 1; Figure 2(b)). Maximum change $\Delta(F\text{-}Gd_{mol} -$

Table 1. DFT computed selected structural parameters of **1** and **1** at various OEEF.

	Complex with EF	Cr–F(Å) (terminal)	Cr–F(Å) (bridged)	F–Gd (Å)	F–Cr–F (°)	Cr–F–Gd (°)
1	**1**	1.844	1.904	2.349	179.3	178.3
2	$\mathbf{1}_{x+0.4}$	1.857	1.854	2.506	178.8	179.7
3	$\mathbf{1}_{x-0.4}$	1.856	1.855	2.506	178.9	179.8
4	$\mathbf{1}_{x+1}$	1.858	1.853	2.524	177.0	179.3
5	$\mathbf{1}_{x-1}$	1.857	1.854	2.829	177.1	179.5
6	$\mathbf{1}_{x+2}$	1.868	1.836	2.864	173.9	178.6
7	$\mathbf{1}_{x-2}$	1.849	1.854	3.442	173.7	179.5
8	$\mathbf{1}_{z+0.4}$	1.861	1.847	2.499	179.9	179.7
9	$\mathbf{1}_{z-0.4}$	1.852	1.861	2.515	179.9	179.9
10	$\mathbf{1}_{z+1}$	1.869	1.837	2.504	179.9	179.9
11	$\mathbf{1}_{z-1}$	1.847	1.871	2.582	179.9	179.9
12	$\mathbf{1}_{z+2}$	1.883	1.823	2.519	179.9	179.9
13	$\mathbf{1}_{z-2}$	1.849	1.856	3.343	179.9	179.8

F-$Gd_{mol\pm n}$) is observed at −1 and ±2 V/Å (Figure 2(b)). Subsequently, we applied Noodleman broken symmetry approach to calculate the Cr–Gd exchange coupling in all the optimized geometries. Also, we observed a decrease in polarity of the molecule in the presence of OEEF, as can be seen from the electrostatic potential diagram in Figure 2(c)–(d).

The combination of minor variations in the Gd−F−Cr angle and the changes in the Gd−F bond distance influenced the magnetic exchange properties of the complex. Specifically, we observed a reduction in the antiferromagnetic exchange interaction along the ±*x*-axis in the modified structures $\mathbf{1}_{x-2}$ and $\mathbf{1}_{x+2}$ (Table 2; Figure 3(a)). In these structures, the exchange coupling constants $J_{Gd\text{-}Cr}$ were found to be $-0.100\ cm^{-1}$ and $-0.123\ cm^{-1}$, respectively. Despite these modifications reducing antiferromagnetic exchange, the complete transition from antiferromagnetic to ferromagnetic exchange was not achieved. This limitation is attributed to the inherent stability and robust nature of the Gd−F−Cr configuration, which resists significant alteration under the applied electric fields. Particularly, π interaction between F and Cr(III) ion, however weak, resist substantial change both in F–Cr distance and the Gd–F–Cr angle. As some of us have previously stated, the decrease in the ∠CrFGd leads to the switch in the exchange coupling, but this switch from antiferromagnetic to ferromagnetic exchange happens at the $\angle CrFGd_{mol}$ of 140°.[25] Unfortunately, the application of OEEF does not alter this angle significantly to see such a drastic change in sign. Hence, we have not observed the switch; the maximum reduction of the exchange from -0.960 to $-0.100\ cm^{-1}$ is observed at −2 V/Å.

3.1 *Mechanism of magnetic exchange in {3d–4f} complexes in the presence of OEEF*

The application of an OEEF alters the magnetic exchange interaction in the Cr–Gd system by modifying key structural parameters, such as the Cr–F and F–Gd bond lengths, as well as the Cr–F–Gd bond angle. Understanding the mechanism by which this coupling is affected under different field conditions is crucial, as it provides insights into how the external electric field influences the exchange interaction through geometric distortions and variations in orbital interactions. In a general {3d–4f} pair, the nature of the exchange interaction is governed by the overlap between the 3d and 4f orbitals. Orthogonality between these orbitals results in ferromagnetic (J_F) contributions, whereas non-vanishing overlap between SOMOs leads to antiferromagnetic (J_{AF}) contributions. Additionally, charge transfer (CT) excitations from the 3d orbital of the Cr^{III} to an empty 5d orbital of the lanthanide contribute to J_F. In complex **1**, the unpaired electrons on Cr^{III} occupy the t_{2g} orbitals (d_{xy}, d_{xz}, d_{yz}), which exhibit π-character, limiting efficient σ-type charge transfer from Cr^{III} to Gd^{III}. As a result, the J_F component is significantly reduced, making J_{AF} a more dominant contribution to the overall exchange interaction (Scheme 1).

Upon applying an external electric field, structural distortions are introduced, particularly affecting the Cr–F and F–Gd bond lengths. These distortions, in turn, modulate the overlap between the Cr^{III} t_{2g} and Gd^{III} 4f orbitals, thereby influencing the magnitude of J_{AF}. In the absence of an electric field (**1**), the system exhibits a relatively strong antiferromagnetic coupling ($J = -0.960\ cm^{-1}$). As the field is applied along the X direction, the F–Gd bond length undergoes elongation,

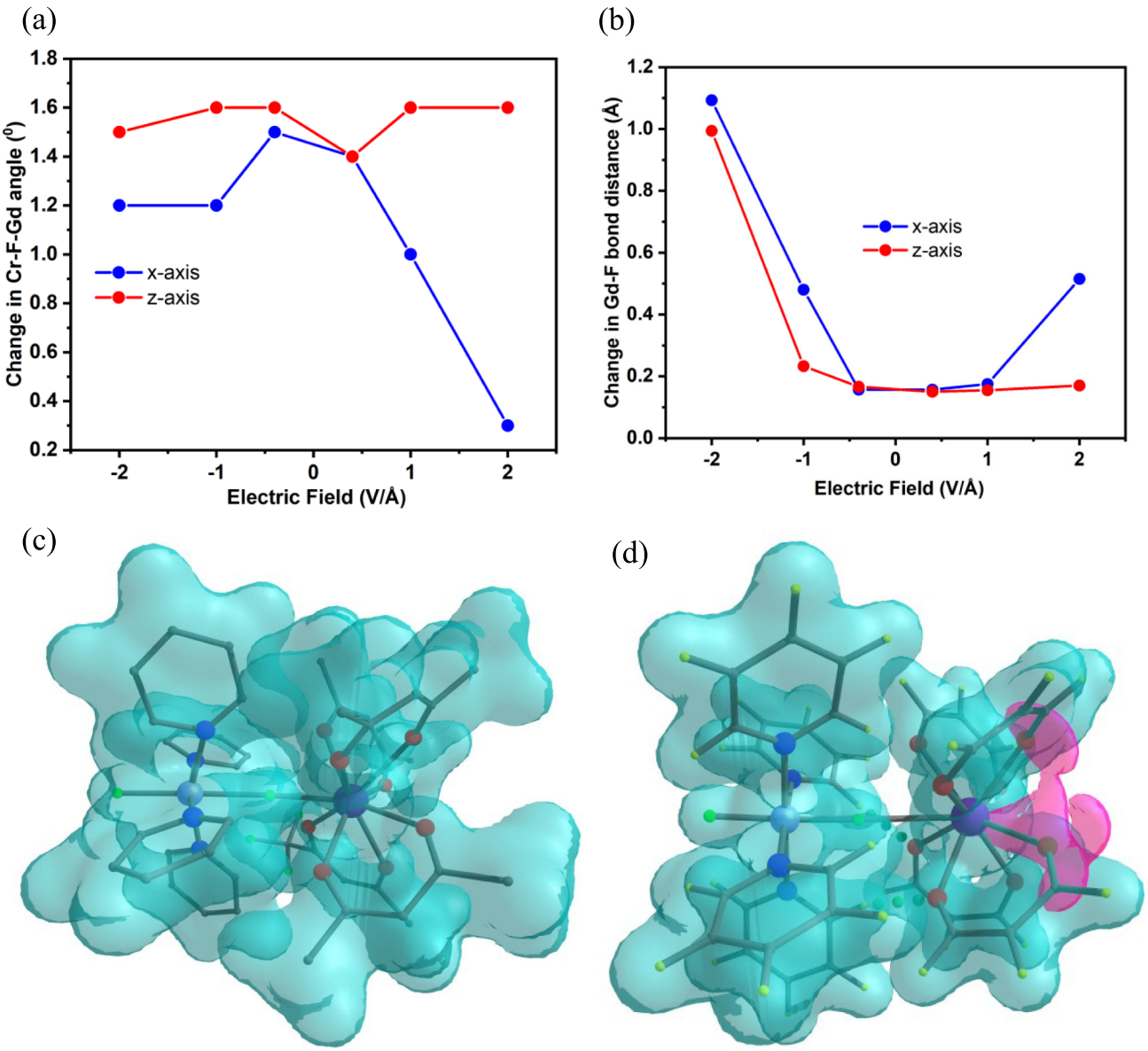

Figure 2. Graph showing changes in (**a**) Gd−F−Cr bond angle for all the geometries optmized in the presence of OEEF with respect to **1**, and (**b**) Gd−F bond length for all the geometries optmized in the presence of OEEF with respect to **1**. (**c**) Computed electrostatic potential diagram of **1** and (**d**) $\mathbf{1}_{x+2}$. Blue and magenta sections show the positive and negative regions of the molecules, respectively.

particularly under negative fields (–X), where it reaches 3.442 Å at −2 V/Å. This increased separation between Gd^{III} and the fluoride bridge weakens the direct {3d–4f} orbital overlap, thereby reducing the magnitude of J_{AF}. Consequently, a sharp decline in antiferromagnetic coupling is observed, with J decreasing to $-0.100\ cm^{-1}$ at −2 V/Å. A similar trend is observed along +X direction, where the F–Gd bond elongates to 2.864 Å at +2 V/Å, resulting in a reduction of J_{AF} to $-0.123\ cm^{-1}$. This reduction in J_{AF} is consistent with a diminished overlap integral between Cr^{III} and Gd^{III}, as well as a reduced charge transfer contribution from Cr^{III} to Gd^{III}, both of which are critical for sustaining antiferromagnetic exchange interactions.

In contrast, when the electric field is applied along the Z direction, distinct effects are observed. The Cr–F (bridged) bond length exhibits contractions under +Z, whereas it elongates under –Z. However, the most significant effect is again observed in the F–Gd bond, which increases to 3.343 Å at −2 V/Å. This elongation weakens the 3d–4f overlap, leading to a drastic reduction in J_{AF}. For moderate field strengths along Z, the J_{AF} contribution steadily declines, with J values of

Table 2. DFT computed exchange coupling constants in various geometries optimised at different electric fields in **1**.

	Field	J_{Cr-F} (cm^{-1})
1	**1**	−0.960
2	$\mathbf{1}_{x+0.4}$	−0.542
3	$\mathbf{1}_{x-0.4}$	−0.542
4	$\mathbf{1}_{x+1}$	−0.506
5	$\mathbf{1}_{x-1}$	−0.507
6	$\mathbf{1}_{x+2}$	−0.123
7	$\mathbf{1}_{x-2}$	−0.100
8	$\mathbf{1}_{z+0.4}$	−0.555
9	$\mathbf{1}_{z-0.4}$	−0.525
10	$\mathbf{1}_{z+1}$	−0.544
11	$\mathbf{1}_{z-1}$	−0.406
12	$\mathbf{1}_{z+2}$	−0.508

−0.555 cm^{-1} at +0.4 V/Å and −0.525 cm^{-1} at −0.4 V/Å, suggesting a progressive weakening of the exchange interaction with increasing field strength.

From an orbital perspective, the electric field influences the relative energies of the Cr^{III} t_{2g} and Gd^{III} 4f orbitals. The application of OEEF increases the electrostatic potential experienced by Gd^{III} (Figure 2(c)–(d); Scheme 1), stabilizing its 4f orbitals. This stabilization further reduces the overlap between the 3d and 4f orbitals, leading to a decrease in J_{AF}. Additionally, it lowers the polarization of the 5d orbitals, resulting in a reduction in J_F. At the same time, the shift in the Cr–F bond modifies the ligand field around Cr^{III}, altering the splitting of its t_{2g} orbitals. Consequently, the energy gap between the 3d and 5d orbitals increases, enhancing charge transfer excitations that contribute to J_F. Furthermore, changes in the Cr–F–Gd bond angle affect the spatial orientation of the orbitals, further reducing the effective overlap necessary for strong J_{AF} interactions.

The application of an external electric field effectively modulates the exchange interaction in the Cr–Gd system by altering key geometric parameters, orbital overlaps, and charge transfer contributions. Fields applied in the X and Z directions elongate the F–Gd bond, weakening the 3d–4f exchange pathway and reducing J_{AF}. Additionally, the splitting of t_{2g} orbitals enhances charge transfer from 3d to 5d orbitals, increasing J_F. Meanwhile, the stabilization of 4f orbitals reduces the polarization of 5d orbitals, leading to a decrease in J_F. However, the overall effect of these factors results in an increase in J_F, thereby reducing the antiferromagnetic exchange under the influence of the electric field. The stronger response observed under –X and –Z fields suggests an asymmetric system reaction, with negative fields more effectively destabilizing the exchange interaction. This tunability of J under an applied field offers valuable insights for designing electric-field-responsive

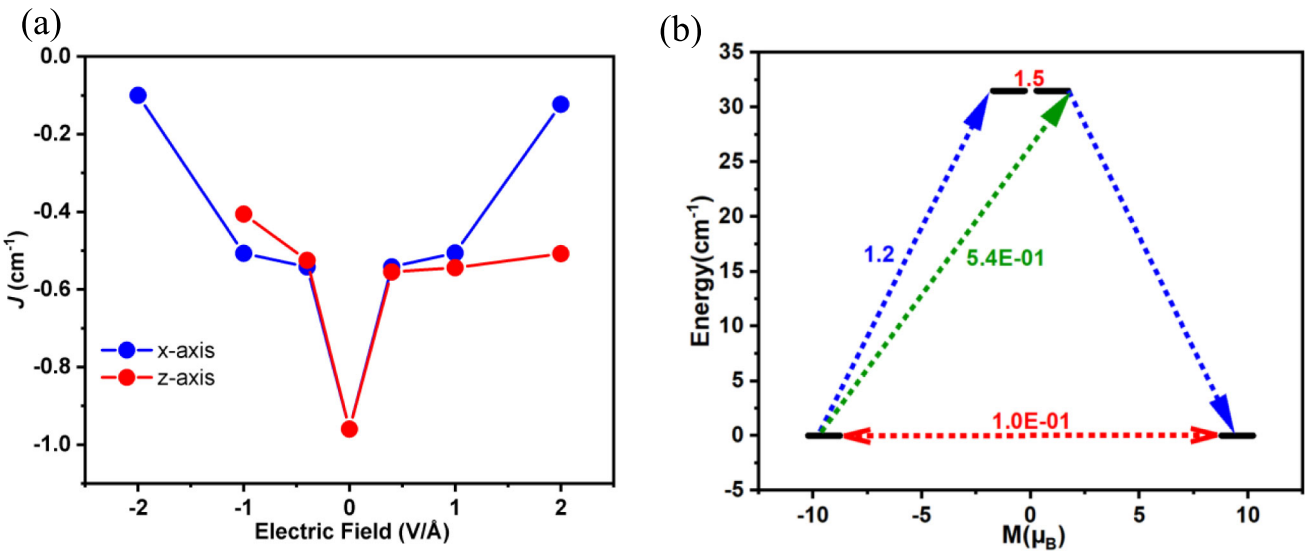

Figure 3. (**a**) Plot between J_{Gd-Cr} and OEEF employed, (**b**) *Ab initio* computed magnetization blockade barrier diagram of **2**. The *x*-axis indicates the magnetic moment of each state along the main magnetic axis while *y*-axis denotes the energy of the respective states. The thick black line indicates the KDs as a function of computed magnetic moment. The green/blue arrows show the possible pathway through Orbach/Raman relaxation. The dotted red lines represent the presence of quantum tunneling mechanism (QTM)/thermally assisted quantum tunneling mechanism (TA-QTM) between the connecting pairs. The numbers provided at each arrow are the mean absolute values for the corresponding matrix element of the transition magnetic moment.

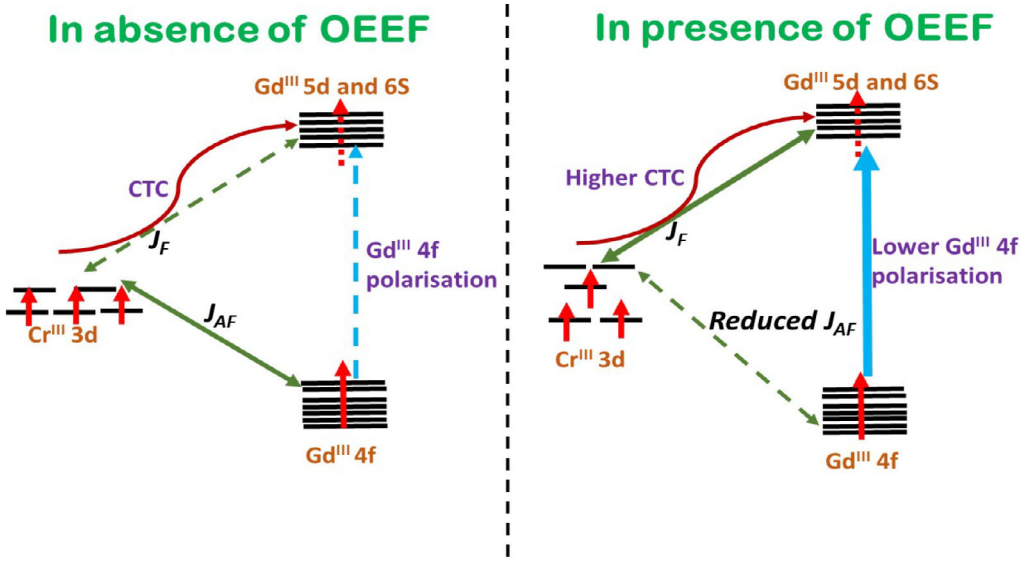

Scheme 1. A schematic mechanism for the magnetic coupling on the [Cr–Gd] pair in the presence and absence of OEEF.

molecular magnets, where controlled modulation of exchange interactions could be harnessed for applications in quantum computing and spintronic devices.

3.2 *Magnetic anisotropy in [$CrF_2(py)_4$]Dy(hfac)$_4$]*

To investigate the magnetic properties of **2**, the Dy^{III} analogue of **1**, we performed CASSCF/RASSI-SO/SINGLE_ANISO calculations. For complex **1**, the first Kramers doublet (KD) lies at 31.5 cm^{-1}, and the overall separation between all Kramers doublets is 244.7 cm^{-1} (refer to Table S1 and Figure 3(b)). The computed g-tensor values reveal significant g_{xx} and g_{yy} components, which deviate from the ideal axial symmetry required for optimal SMM behaviour. Although the QTM within the ground state is minimal, the presence of TA-QTM facilitates relaxation from the first excited state, thereby limiting the effective energy barrier to 31.5 cm^{-1}.

For the system $\mathbf{1}_{x+2}$, a decrease in antiferromagnetic exchange was expected to suppress QTM and thereby enhance the overall magnetic performance. However, despite this expectation, the g_{xx} and g_{yy} values remain significant, suggesting a persistent deviation from strong uniaxial anisotropy. Additionally, the energy of the first excited state in $\mathbf{1}_{x+2}$ is 29.4 cm^{-1}, which is nearly identical to that of **1**. Interestingly, we observed a notable increase in the overall crystal field splitting, which is 324.1 cm^{-1} for $\mathbf{1}_{x+2}$, compared to 244.7 cm^{-1} in **1**. This increase in crystal field splitting suggests that while the electronic environment is altered, it does not necessarily translate into an improved SMM performance due to the significant transverse anisotropy. Therefore, one has to choose the system carefully, particularly with ligands that are flexible to modulate the behaviour under the EF.

4. Conclusions

This study systematically investigates the influence of OEEF on the structural and magnetic properties of lanthanide-based SMMs, with a focus on Cr–Gd and Cr–Dy complexes. Through a combination of DFT and *ab initio* calculations, we addressed key questions regarding how OEEF affects magnetic exchange interactions, co-ligand influences, and the potential for tuning exchange couplings through external perturbations.

Impact of OEEF on structural parameters and magnetic exchange (J values): Our findings demonstrate that the application of an electric field along the X and Z directions induces significant geometric modifications, particularly in Cr–F (terminal and bridged) and F–Gd bond lengths, as well as minor variations in the Cr–F–Gd bond angle. Notably, the F–Gd bond elongates dramatically under negative X and Z fields, weakening the super-exchange interaction and reducing the antiferromagnetic exchange constant from −0.960 cm^{-1} to −0.100 cm^{-1} at −2 V/Å. These results highlight the tunability of magnetic interactions through structural distortions induced by OEEF.

Role of co-ligand in modulating magnetic exchange: The choice of co-ligands plays a crucial role in

defining the electronic environment and influencing exchange interactions. Modifications in the ligand field alter the spatial distribution of 3d–4f orbital overlap, affecting charge transfer (CT) excitations and exchange contributions. While OEEF influences bond distances and orbital overlap, the co-ligand remains a fundamental factor in determining the nature and strength of the magnetic exchange within these complexes.

Potential for reversing the sign of magnetic exchange via OEEF: Although the application of OEEF significantly weakens antiferromagnetic interactions, a complete transition to ferromagnetic exchange was not observed. This is primarily due to the robust structural stability of the Gd–F–Cr bridge, which resists large angular distortions necessary for a J sign reversal. Prior studies suggest that an exchange switch occurs at a Cr–F–Gd angle of $\sim 140°$, but OEEF-induced distortions were insufficient to reach this threshold. This suggests that while OEEF effectively modulates J, additional chemical modifications, such as ligand engineering or external pressure, may be required to achieve a ferromagnetic ground state.

Tuning magnetic anisotropy in Dy^{III} complexes: To extend this approach beyond Gd^{III} (isotropic) systems, we conducted RASSCF/RASSI/SINGLE_ANISO calculations for Dy^{III}-based SMMs. Our analysis reveals that while the first KD in $\mathbf{1}_{x+2}$ lies at 29.4 cm^{-1}, similar to **1** (31.5 cm^{-1}), the overall crystal field splitting increases to 324.1 cm^{-1} (compared to 244.7 cm^{-1} in **1**). However, despite this increase, significant g_{xx} and g_{yy} components persist, indicating strong transverse anisotropy, which limits improvements in SMM performance. These results suggest that while OEEF influences structural parameters, its direct impact on improving Dy^{III}-based SMM behaviour is constrained by the system's inherent electronic anisotropy.

The ability to modulate magnetic exchange interactions via external electric fields provides a powerful tool for designing field-responsive molecular magnets.

Acknowledgements

TS thanks CSIR India for funding. GR would like to thank SERB (SB/SJF/2019-20/12; CRG/2022/001697) for funding.

Funding

Serb, CRG/2018/000430, G. Rajaraman, DST/SJF/CSA03/2018-10; SB/SJF/2019-20/12, G. Rajaraman.

References

1. Sessoli R and Powell A K 2009 Strategies towards single molecule magnets based on lanthanide ions *Coord. Chem. Rev.* **253** 2328–2341
2. Vieru V, Gómez-Coca S, Ruiz E and Chibotaru L F 2024 Increasing the magnetic blocking temperature of single-molecule magnets *Angew. Chem.* **136** e202303146
3. Swain A, Sharma T and Rajaraman G 2023 Strategies to quench quantum tunneling of magnetization in lanthanide single molecule magnets *Chem. Commun.* **59** 3206–3228
4. Eliseeva S V, Ryazanov M, Gumy F, Troyanov S I, Lepnev L S, Bünzli J C G *et al.* 2006 Dimeric complexes of lanthanide(III) hexafluoroacetylacetonates with 4-cyanopyridine N-oxide: synthesis, crystal structure, magnetic and photoluminescent properties. *Eur. J. Inorg. Chem.* 4809-4820
5. Ahmed N, Sharma T, Spillecke L, Koo C, Ansari K U, Tripathi S *et al.* 2022 Probing the origin of ferro-/antiferromagnetic exchange interactions in Cu (II)–4f complexes *Inorg. Chem.* **61** 5572–5587
6. Schmidt S F, Merkel M P, Kostakis G E, Buth G, Anson C E and Powell A K 2017 SMM behaviour and magnetocaloric effect in heterometallic 3d–4f coordination clusters with high azide: metal ratios *Dalton Trans.* **46** 15661–15665
7. Wang H S, Zhang K, Song Y and Pan Z Q 2021 Recent advances in 3d–4f magnetic complexes with several types of non-carboxylate organic ligands *Inorg. Chim. Acta.* **521** 120318
8. Ma Y Z, Zhang L M, Peng G, Zhao C J, Dong R T, Yang C F and Deng H 2014 A series of three-dimensional 3d–4f cyanide heterometallic coordination polymers: synthesis, crystal structure, photoluminescent and magnetic properties *Cryst. Eng. Comm.* **16** 667–683
9. Maurice R, Mallah T and N Guihéry 2023 In *Modes of Cooperative Effects in Dinuclear Complexes* Kalck P (ed.) (Springer) p. 207-233
10. Aragones A C, Haworth N L, Darwish N, Ciampi S, Bloomfield N J, Wallace G G *et al.* 2016 Electrostatic catalysis of a Diels-Alder reaction *Nature* **531** 88–91
11. Bleuzen A, Marvaud V, Mathoniere C, Sieklucka B and Verdaguer M 2009 Photomagnetism in clusters and extended molecule-based magnets *Inorg. Chem.* **48** 3453–3466
12. Hoffmann S, Goslar J, Hilczer W and Krupski M 1993 Pressure-induced temperature dependence of a weak exchange coupling in dichlorobis (1-phenyl-3, 5-dimethylpyrazole) copper (II) crystals *Inorg. Chem.* **32** 3554–3556
13. Cui Y, Wu Y, Li Y, Liu R, Dong X and Wang Y 2014 Pressure-induced changes in the magnetic properties of the single crystal of Mn_3 single-molecule magnet *Sci. China Phys Mech. Astro.* **57** 1299–1303
14. Fittipaldi M, Cini A, Annino G, Vindigni A, Caneschi A and Sessoli R 2019 Electric field modulation of magnetic exchange in molecular helices *Nat Mater.* **18** 329–334
15. Palii A, Tsukerblat B, Klokishner S, Aldoshin S, Korchagin D and Clemente-Juan J M 2018 Electric

field control of spin states in trigonal two-electron quantum dot arrays and mixed-valence molecules: I. Electronic problem *J. Phys. Chem. C* **123** 2451–2459
16. Sarkar A and Rajaraman G 2020 Modulating magnetic anisotropy in Ln(III) single-ion magnets using an external electric field *Chem. Sci.* **11** 10324–10330
17. Tiwari R K, Paul R and Rajaraman G 2024 Investigating the influence of oriented external electric fields on modulating spin-transition temperatures in Fe (ii) SCO complexes: a theoretical perspective *Dalton Trans.* **53** 14623–14633
18. Sharma T, Singh A and Rajaraman G 2025 Effect of oriented external electric field in altering magnetic exchange and magnetic anisotropy in lanthanide-radical complexes *Chem. Eur. J.* **31** e202402868
19. Goodwin C A, Ortu F, Reta D, Chilton N F and Mills D P 2017 Molecular magnetic hysteresis at 60 kelvin in dysprosocenium *Nature* **548** 439–442
20. Guo F S, Day B M, Chen Y C, Tong M L, Mansikkamäki A and Layfield R A 2018 Magnetic hysteresis up to 80 kelvin in a dysprosium metallocene single-molecule magnet *Science* **362** 1400–1403
21. Gould C A, McClain K R, Reta D, Kragskow J G, Marchiori D A, Lachman E *et al.* 2022 Ultrahard magnetism from mixed-valence dilanthanide complexes with metal-metal bonding *Science* **375** 198–202
22. Lescop C, Belorizky E, Luneau D and Rey P 2002 Synthesis, structures, and magnetic properties of a series of lanthanum(III) and gadolinium(III) complexes with chelating benzimidazole-substituted nitronyl nitroxide free radicals. Evidence for antiferromagnetic Gd^{III}-radical interactions *Inorg. Chem.* **41** 3375–3384
23. Zhao H, Bazile J, Mervin J, Galán-Mascarós J R and Dunbar K R 2003 A rare-earth metal TCNQ magnet: synthesis, structure, and magnetic properties of $\{[Gd_2(TCNQ)_5(H_2O)_9][Gd(TCNQ)_4(H_2O)_3]\}\cdot 4H_2O$ *Angew. Chem. Int. Ed.* **42** 1015–1018
24. Dreiser J, Pedersen K S, Piamonteze C, Rusponi S, Salman Z, Ali M E *et al.* 2012 Direct observation of a ferri-to-ferromagnetic transition in a fluoride-bridged 3d–4f molecular cluster *Chem. Sci.* **3** 1024–1032
25. Singh S K, Pedersen K S, Sigrist M, Thuesen C A, Schau-Magnussen M, Mutka H *et al.* 2013 Angular dependence of the exchange interaction in fluoride-bridged Gd^{III}–Cr^{III} complexes *Chem. Commun.* **49** 5583–5585
26. Frisch M et al. 2009 Gaussian 09, Revision d. 01, Gaussian, *Inc, Wallingford CT* **201**.
27. Becke A D 1988 Density-functional exchange-energy approximation with correct asymptotic behavior *Phys. Rev. A* **38** 3098
28. Lee C, Yang W and Parr R G 1988 Development of the Colle-Salvetti correlation-energy formula into a functional of the electron density *Phys. Rev. B* **37** 785
29. Becke A D 1992 Density-functional thermochemistry. I. The effect of the exchange-only gradient correction *J. Chem. Phys.* **96** 2155–2160
30. Cundari T R and Stevens W J 1993 Effective core potential methods for the lanthanides *J. Chem. Phys.* **98** 5555–5565
31. Dolg M, Wedig U, Stoll H and Preuss H 1987 Energy-adjusted ab initio pseudopotentials for the first row transition elements *J. Chem. Phys.* **86** 866–872
32. Aquilante F, Autschbach J, Carlson R K, Chibotaru L F, Delcey M G, De Vico L *et al.* 2016 Molcas 8: New capabilities for multiconfigurational quantum chemical calculations across the periodic table *J. Comput. Chem.* **37** 506–541
33. Roos B R O, Lindh R, Malmqvist P A, Veryazov V, Widmark P O and Borin A C 2008 New relativistic atomic natural orbital basis sets for lanthanide atoms with applications to the Ce diatom and LuF_3 *J. Phys. Chem. A* **112** 11431–11435
34. Nakajima T and Hirao K 2012 The Douglas–Kroll–Hess approach *Chem. Rev.* **112** 385–402
35. Ungur L and Chibotaru L F 2017 Ab initio crystal field for lanthanides *Chem. Eur. J.* **23** 3708–3718
36. Chibotaru L F and Ungur L 2012 Ab initio calculation of anisotropic magnetic properties of complexes. I. Unique definition of pseudospin Hamiltonians and their derivation *J. Chem. Phys.* **137**